Available online at www.sciencedirect.com
SCIENCE DIRECT®
ELSEVIER
Nuclear Instruments and Methods in Physics Research A 545 (2005) 542–553
NUCLEAR INSTRUMENTS & METHODS IN PHYSICS RESEARCH Section A
www.elsevier.com/locate/nima

Neutral beam line to study $K_L^0 \to \pi^0 \nu\bar{\nu}$ decay at the KEK 12-GeV proton synchrotron

H. Watanabe[a,*], K. Abe[b], Y. Aikawa[b], Y. Akune[b], M. Doroshenko[c], E. Harada[b], Y.B. Hsiung[d], T. Ikei[e], Y. Ikemoto[e], S. Inoue[b], T. Inagaki[c], N. Kawakubo[b], S. Kobayashi[b], T. Kojima[b], A.S. Kurilin[f], S.Y. Lee[g], G.Y. Lim[c], J. Nix[a], I. Ogawa[b], H. Okuno[c], K. Omata[c], T. Oba[e], G.N. Perdue[a], K. Sakashita[e], T. Sato[c], T. Shinkawa[h], Y. Sugaya[e], T. Sumida[i], Z. Tsamalaidze[f], T. Tsukamoto[b], Y.W. Wah[a], M. Yamaga[c], T. Yamanaka[e], Y. Yoshimura[c]

[a]*Enrico Fermi Institute, University of Chicago, Chicago 60637, USA*
[b]*Department of Physics, Saga University, Saga 840-8502, Japan*
[c]*High Energy Accelerator Research Organization, KEK, Ibaraki 305-0801, Japan*
[d]*Fermi National Accelerator Laboratory, IL 60510, USA*
[e]*Department of Physics, Osaka University, Osaka 560-0043, Japan*
[f]*Joint Institute for Nuclear Research, 141980 Dubna, Moscow region, Russian Federation*
[g]*Department of Physics, Pusan National University, Pusan, 609-735, Korea*
[h]*National Defense Academy in Japan, Kanagawa 239-8686, Japan*
[i]*Department of Physics, Kyoto University, Kyoto 606-8502, Japan*

Received 23 November 2004; received in revised form 8 February 2005; accepted 8 February 2005
Available online 8 April 2005

Abstract

A neutral beam line was constructed at the 12-GeV proton synchrotron of KEK for an experiment to study $K_L^0 \to \pi^0 \nu\bar{\nu}$ decay. It was designed to make a well-collimated K_L^0 beam with small γ and neutron halos. In a series of beam-survey experiments, beam profiles and energy spectra of γ's and neutrons were measured. It was confirmed that the beam was sharply collimated with a halo-to-core flux ratio lower than 10^{-4}. These experimental results were well reproduced by a Monte-Carlo simulation based on the GEANT-3 program.

PACS: 29.25

Keywords: Neutral beam line; Pencil beam; $K_L^0 \to \pi^0 \nu\bar{\nu}$.

*Corresponding author. KEK Building No. 4, Oho 1-1, Tsukuba 305-0801, Japan. Tel.: +81 298 796042; fax: +81 298 647831.
E-mail address: nabe@post.kek.jp (H. Watanabe).

0168-9002/$ - see front matter © 2005 Elsevier B.V. All rights reserved.
doi:10.1016/j.nima.2005.02.011

1. Introduction

Measuring the $K_L^0 \to \pi^0\nu\bar{\nu}$ decay branching ratio is one of the most important clues to clarify the origin of CP violation in elementary-particle physics [1]. The KEK-E391a experiment aims to measure this branching ratio at a single event sensitivity of 3×10^{-10} [2,3]. The present experimental upper limit is 5.9×10^{-7} [4], which is far from the Standard-Model prediction of 3×10^{-11} [1].

Experimentally, the identification of this very rare $K_L^0 \to \pi^0\nu\bar{\nu}$ decay is not definite because the decay kinematics can not be uniquely determined. In order to reject many backgrounds due to other K_L^0 decays and due to the beam-associated π^0 production, a specially designed neutral beam line as well as a highly hermetic photon detector are necessary [2].

A neutral beam line, which produces a well-collimated "pencil" beam, was constructed for the E391a experiment in the east counter hall at the KEK 12-GeV proton synchrotron. A series of beam-survey experiments were carried out in April, December 2000 and December 2001, and the experimental data were compared with a Monte-Carlo simulation based on the GEANT-3 program [5].

2. Neutral beam line

A neutral beam line consists of a platinum target, a pair of sweeping magnets, two stages of collimation using six sets of collimators (C1–C6), lead(Pb) and beryllium(Be) absorbers and a vacuum pipe, as shown in Fig. 1.

2.1. Basic concept of the design

In order to detect a unique kinematical signature for the $K_L^0 \to \pi^0\nu\bar{\nu}$ decay by using a transverse momentum and an acoplanarity angle of two photons, the most essential requirement is a well-collimated "pencil" beam with a minimum halo.

The basic concepts of the design are:

(1) A neutral beam line is set at 4° with respect to the primary proton beam hitting the platinum target. The mean of K_L^0 momentum is 3.5 GeV/c at the target.
(2) The total length of the beam line is 10 m in order to reduce hyperons in the beam and to reduce punching-through muons.
(3) The first three collimators (C1, C2, C3) are used to define the beam profile in an aperture of 2 mrad of a half-cone angle.
(4) The last two collimators (C5, C6) are used to trim the beam halo.
(5) Movable Pb/Be absorbers are prepared to control the neutron and γ fluxes relative to the K_L^0 flux.
(6) Two dipole magnets are installed to sweep out charged particles.
(7) The downstream half of last collimator (C6) also acts as an active collimator using scintillators in order to veto background events produced by the beam halo at that place.
(8) Thin Gd_2O_3 sheets are placed in the fourth collimator (C4) to reduce thermal neutrons.
(9) The downstream half of the beam line is kept in vacuum of 1-Pa level, and it is connected to fiducial decay region through thin membrane at the exit of the beam line. The vacuum level inside the fiducial decay region is 10^{-5} Pa level.

Details are described in the following sections.

2.2. Primary proton beam and K_L^0 production target

Primary protons with a kinetic energy of 12 GeV hit the production target made of platinum(Pt) with 60 mm thickness ($0.68\lambda_I, 20X_0$) and 8 mm diameter. The profile of the primary proton beam is an ellipse with $\sigma = 1.1$ mm vertically and $\sigma = 3.3$ mm horizontally, as shown in Fig. 2. It was measured by detecting heat from a wire moving across the beam, as described in Ref. [6]. The target was inclined by 4° horizontally with respect to the primary beam axis. In order to promptly absorb non-interacting primary protons and high-energy secondaries, we installed a 25 cm-thick beam plug made of tungsten ($2.6\lambda_I$, $71X_0$) into the primary beam dump. Both the first collimator C1 and the beam dump start at 80 cm from the target.

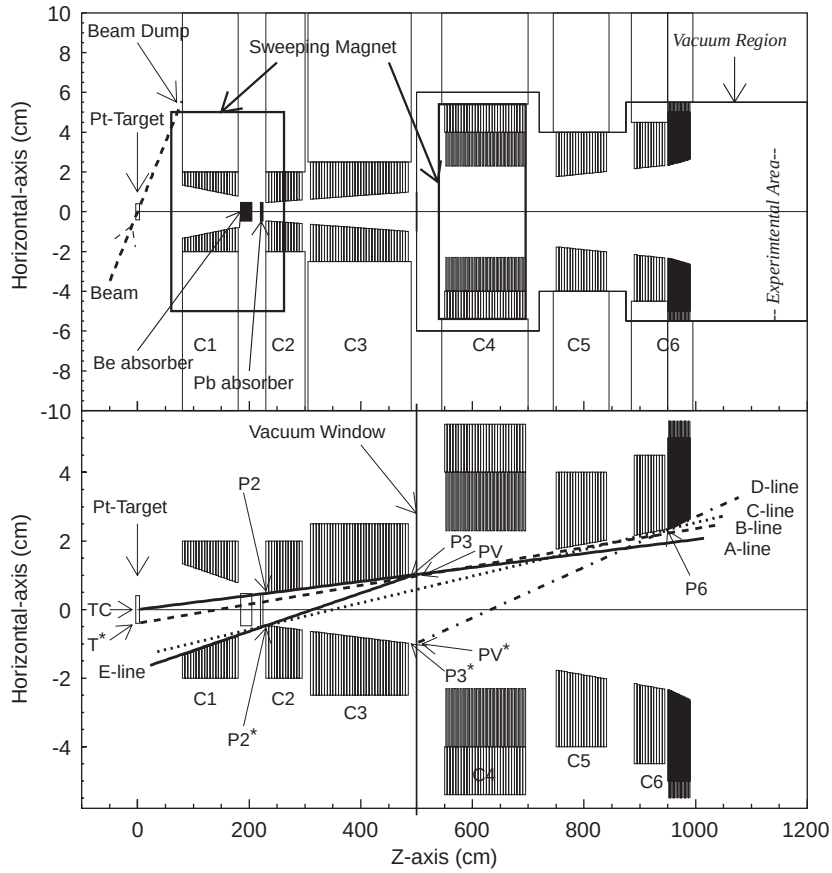

Fig. 1. Schematic views of the neutral beam line. The top figure shows the arrangement of the beam-line components. The bottom figure shows the collimation scheme. In the bottom figure, solid lines indicate A-line and E-line, a dashed line indicates B-line, a dotted line indicates C-line and a dashed-and-dotted line indicates D-line.

2.3. Collimation scheme

The bottom figure in Fig. 1 shows the beam-collimation scheme. Cylindrical disks of 5 cm-thick tungsten are arranged to approximate the lines indicated in the bottom figure of Fig. 1. All of the disks are kept in steel pipes, and these pipes are supported by brass structures. Outside of these parts, steel, heavy concrete and ordinary concrete shields are piled. Here, C1, C2, C3, C4, C5 and C6 in the figure indicate collimators 1–6, respectively. The symbols TC and T* indicate the target center and the edge point of the target, respectively. The symbols P2, P3, PV and P6 indicate the edge points of the entrance of C2, the exit of C3, the vacuum window just after C3 and the middle of C6, respectively. The symbols with an asterisk(*) show the opposite sides with respect to the beam axis.

- *A-line* is drawn as a line of the 2 mrad cone from the target center (TC). The inner surfaces of collimators C2 and C3 are placed along this line and define the core of the beam profile.
- *B-line* is a line connecting T* and P3. C5 and the upstream-half of C6 are arranged along this line. This line shows the penumbra due to the finite size of the target. The aperture of C5 and upstream-half of C6 have a clearance of 0.2 mm with respect to the B-line. Then, the particles produced at the target do not hit C5 and C6 directly.

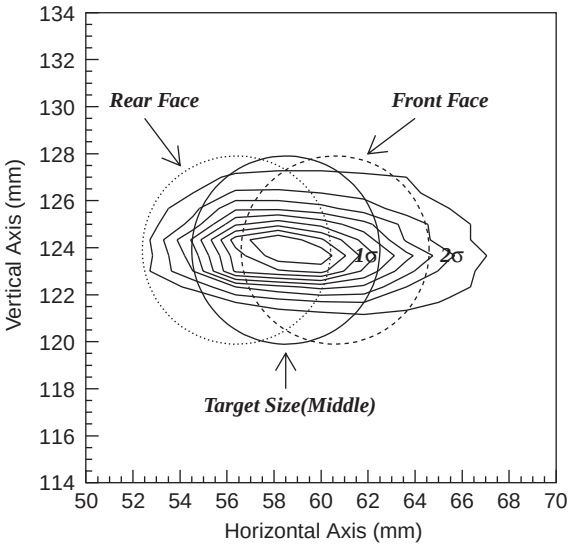

Fig. 2. Beam profile of primary protons at the production target. The circles indicate the target position. The target inclines by 4° with respect to the proton beam direction.

- *C-line* connects P2* and P6. A lead absorber of 5 cm-thick ($8.9X_0$, $0.49\lambda_T$) and a beryllium absorber of 30 cm-thick ($0.85X_0$, $0.99\lambda_T$) are placed between C1 and C2. Since their lateral size is small (1 cm diameter) and they are within the C-line (extrapolated to the upstream direction), the free run-through of the secondaries produced at the absorber are limited in the cone defined by this C-line.
- *D-line* is a line connecting PV* and P6. Since the upstream defining collimators are enveloped in the D-line, it is a boundary for secondaries produced at the defining collimators. It is also a boundary for the secondaries scattered by air before the vacuum region and the window. The tertiaries originated from the secondaries at C1 are also within this envelope, because the acceptance of the secondaries from C1 are limited by the E-line. The latter half of C6 is arranged along the D-line in order to prevent edge scattering of the particles from the tertiaries mentioned above.
- *E-line* connects P2* and P3. The inner surface of C1 is arranged along this line. Secondaries, which are produced at C1, should have a larger angle than the E-line. They direct to the collimator surface more upstream than C3.

In summary, the D-line is a boundary of the beam halo from all secondary beam sources (defining collimators, absorbers, air and the vacuum window) and a tertiary beam source from the hottest collimator C1. More steps of interactions and penetrations through the material might be sources of the wider beam halo.

2.4. Thermal neutron absorber

A large number of thermal neutrons are expected to appear in the detector area through the beam-line hole, which will make the background signals in the detector. Since the beam-defining section(C2–C3) and the halo-trimming section(C5–C6) are already thick enough ($>20\lambda_I$), we installed a thermal-neutron absorber in the C4 region. It is composed of multi-layer disks of a 5 cm-thick brass plate and a 100 μm-thick PET sheet containing gadolinium-oxide(Gd_2O_3) by 40% in weight, as shown in Fig. 3. The total number of disks is 29. The Gd_2O_3 sheet is pasted to an inner surface of the brass plate. The hole of the disk has a diameter of 4.6 cm, which is about 2-times larger than that of the beam profile at the C4 region. The brass structure was used to shield low-energy photons emitted after thermal neutron absorption by gadolinium.

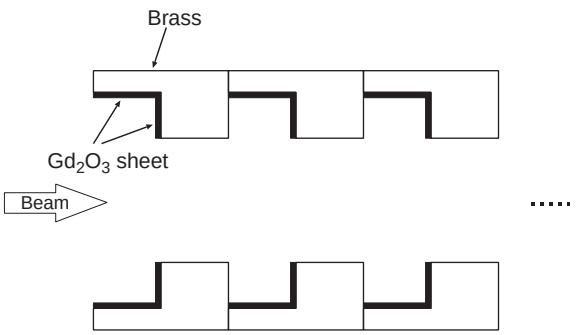

Fig. 3. Schematic view of C4 collimator. A Gd_2O_3 sheet is pasted on the brass collimator, which is used as a thermal neutron absorber.

2.5. Installation of scintillator plates in collimator C6

A part of halo neutrons are produced at C6 by secondary neutrons and by charged pions from K_L^0 decays. In order to reject the background events due to neutrons produced at C6, plastic-scintillator disks of 1 cm thick were installed as an active veto element between the tungsten disks in a downstream-half of C6, as shown in Fig. 4. Scintillation light was read out through wavelength-shifter fibers arranged at the outer periphery of the scintillator disks. It was estimated by a Monte-Carlo simulation that 98% of the halo neutrons produced by K_L^0 decays at C6 can be rejected by C6 signals.

3. Beam-line simulation

A Monte-Carlo simulator of the neutral beam line was developed using the GEANT-3 program [5]. A G-FLUKA [5] code was used as a hadron interaction package. A beam-line simulation was performed in two steps. First was a particle-production stage at the target. We generated primary protons with kinetic energies of 12 GeV on a Pt production target with 60 mm thickness and 8 mm diameter, and collected information about the secondary particles at 7 cm from the target. The elliptical beam profile of primary protons was generated using a Gaussian function with $\sigma = 1.1$ mm in the vertical direction and $\sigma = 3.3$ mm in the horizontal direction, as described in Section 2.2. The threshold energy in the GEANT-3 code was set to be 10 keV. We generated events corresponding to 10^8 protons on the target(pot).

We then started the beam-line simulation from collimators C1 to C6 using the above seed events. Since the number of events for 10^8 pot is not sufficient for a detailed simulation of the beam-halo events, we used the same events 100 times, and obtained 10^{10} pot-equivalent events. In this simulation, the threshold energy was set to be 1 MeV. In order to save CPU time, particles that went out beyond the outside boundaries of the collimators were eliminated. We carried out a simulation under three conditions of the beam-line absorber: no absorber, with the Pb absorber and with the Be absorber.

At the exit of the beam line, most of the beam components were neutrons and γ's. The number of K_L^0's was only 38 per 10^8 pot. Therefore, we performed a special generation of seeds to obtain the K_L^0 energy distribution, in which the threshold energy for neutrons and γ's was set as 1 GeV to save computing time. Fig. 5 shows the momentum distribution of K_L^0's at the exit of the beam line obtained for 10^{10} pot. The number of K_L^0 at the exit of C6 with no absorber and with the Pb absorber were 3113 K_L^0's/10^{10}pot and 2326 K_L^0's/10^{10}pot, respectively. The momentum spectra and beam profiles were obtained from beam-line simulations for γ's and neutrons by multiple usage of seeds, as

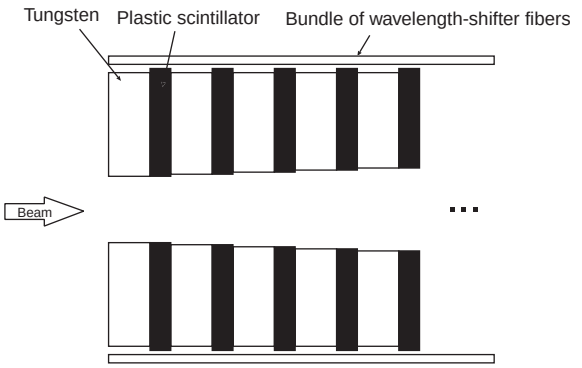

Fig. 4. Schematic view of the active part(downstream-half) of collimator C6, which consists of a sandwich of a 2 cm-thick tungsten plate and a 1 cm-thick scintillator plate.

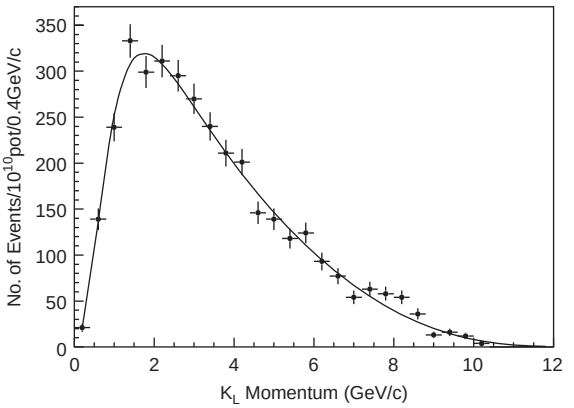

Fig. 5. K_L^0 momentum distribution at the exit of the beam line obtained by the beam-line simulation (no absorber case).

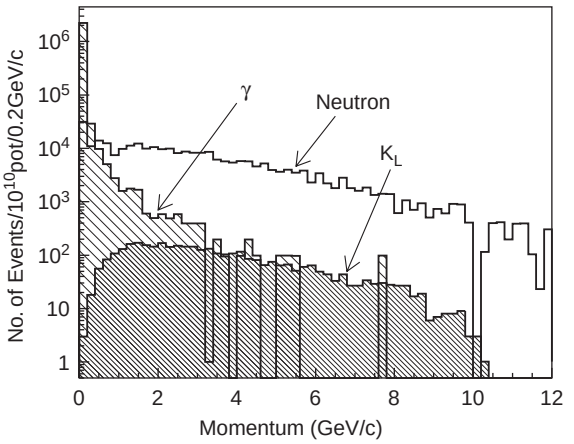

Fig. 6. Momentum distributions at the exit of C6 for γ's and neutrons obtained by the beam-line simulation (no absorber case).

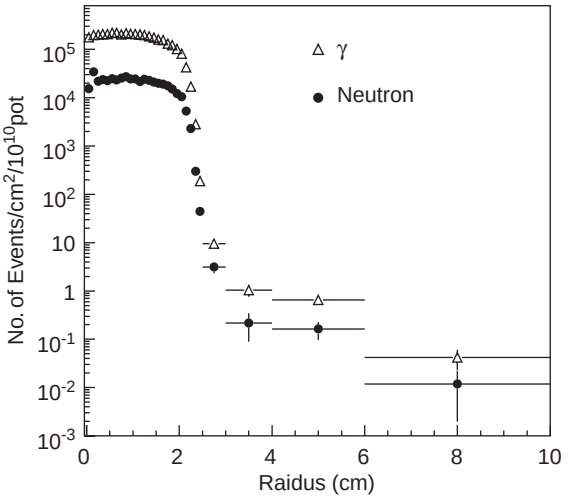

Fig. 7. Beam profiles at the exit of C6 in the energy region above 1 MeV obtained by a beam-line simulation (no absorber case). The triangles and circles indicate those for γ's and neutrons, respectively.

shown in Figs. 6 and 7. The mean value of K_L^0 momentum is 3.5 GeV/c. The n/K_L^0 ratio above 100 MeV was ~60 in a case of no absorber.

4. Beam-survey experiment

We carried out a series of beam-survey experiments in April and December 2000, and December 2001. During the beam survey, the proton flux on the production target was 10^{11} protons per pulse, which was measured with a secondary emission monitor. The pulse repetition rate was 0.25 Hz and the beam spill length was 2 s.

4.1. Beam-profile measurement

4.1.1. Method and apparatus

In order to measure the profiles of γ's, neutrons and charged particles separately, we prepared a counter telescope consisting of a 1 cm-thick plastic scintillator, a 6 cm-thick plastic scintillator ($0.14X_0$, $0.11\lambda_T$) and a lead-scintillator sandwich counter, as shown in Fig. 8. The sandwich counter was composed of 15 layers of 1 mm-thick lead and 5 mm-thick scintillator, and had a total thickness of 9 cm ($2.85X_0$, $0.28\lambda_T$). The cross-section of all the counters was $4 \times 5\,\mathrm{cm}^2$, while the expected cross-section of the beam was a circle of 5 cm diameter. The front face of these counters were located at 1.7 m from the exit of collimator C6. An X–Y stage was used to move the counter telescope with an accuracy of 1 mm.

We named a coincidence between signals of first and second counters as charged particle(C), a signal of the second counter vetoed by the first counter as neutron(N), and a signal of the third counter vetoed by the first counter as γ(G). The energy thresholds were set to be 0.46 MeV for the first counter, 7.32 MeV for the second counter and 8.83 MeV for the third counter. A profile measurement was performed by counting these C, G and N events with scalers.

4.1.2. Results

Fig. 9 shows beam profiles measured in the K0 beam line. The number of events was normalized to 10^{10} protons on the target. In the figure, profiles are shown for the two conditions, with no-absorber and with the Pb-absorber.

(1) The flux in the beam halo region was found to be 10^{-4} of the flux in the beam core region for both G and N.
(2) The Pb-absorber reduces the overall flux by one order of magnitude.

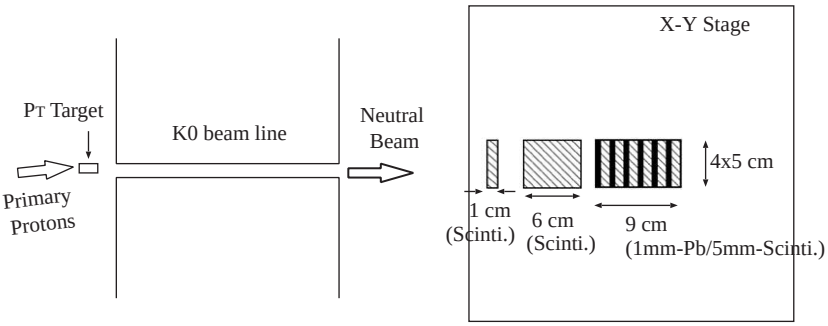

Fig. 8. Schematic view of the setup for the beam-profile measurements.

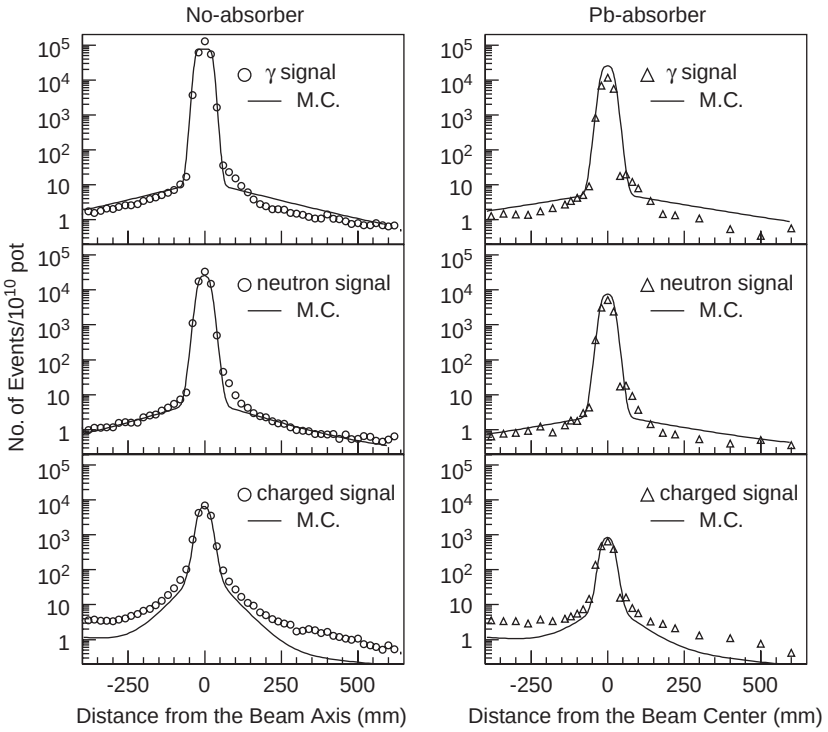

Fig. 9. Beam profiles. The left-side figures with open circles indicate the data for the no-absorber case, and the right-side figures with triangles indicates the data for the Pb-absorber case. The solid lines show results of the Monte-Carlo simulation.

Simulation results, which include detector responses, are shown by the solid lines in Fig. 9. One of the important corrections for the detector efficiencies is a size effect of the telescope, and the other is detection efficiencies for various particles. Table 1 shows a typical efficiency estimated from the detector simulation. Actually, the effects of size and efficiencies were corrected event by event. Data and the simulation results show a reasonably good agreement, as shown in Fig. 9. Especially, the sharp edges were well reproduced by the simulation. The size of the beam core, which was smeared by the detector-size effect, was 3.70 cm (FWHM) for the data, and it is 3.72 cm for the simulation.

Table 1
Typical detection efficiencies of the counter telescope, estimated by a simulation based on the GEANT-3 program

	Incident particle		
	Charged(μ^-) (%)	Neutron (%)	γ (%)
C	100	0.55	1.3
N	<0.1	5.8	6.6
G	<0.1	15.4	81.0

Particles were generated at the center of the detector with a kinetic energy of 1.0 GeV. Definitions of each output are written in the text.

However, a discrepancy was seen in the number of charged particles in the halo region. This discrepancy might be due to μ's that punched through concrete shields surrounding the beam line.

4.2. Spectrum measurements for γ and n

4.2.1. Method and apparatus

Energy distributions of the γ's and the neutrons were measured with a hadron calorimeter, named Cerberus, as shown in Fig. 10. It consisted of 6 modules, each having a cross-section of $40 \times 40\,\mathrm{cm}^2$ and a thickness of 20 cm. The front module consisted of 25-layers of 4 mm-thick lead and 3.7 mm-thick scintillator plates sandwiched with each other. The radiation length and the nuclear interaction length of the front module were $18X_0$ and $0.7\lambda_I$, respectively. For the other 5 modules, which are called "rear modules", 4 mm-thick iron plates were used as a converter. The total nuclear interaction length of Cerberus was $4.27\lambda_I$. Two plastic scintillators were placed in front of Cerberus. In order to achieve a good uniformity of a light-collection efficiency, 8 PMTs per module were used to read out scintillation light through 10 cm-thick Lucite light guides from the up and down sides. At a trigger stage, we requested signals in any of the rear 5 modules for neutrons, and a signal in the first module for γ. In both cases, the front two scintillators were used for a veto. We also collected charged-particle events for gain monitoring by requesting a coincidence of the first module and the front scintillators.

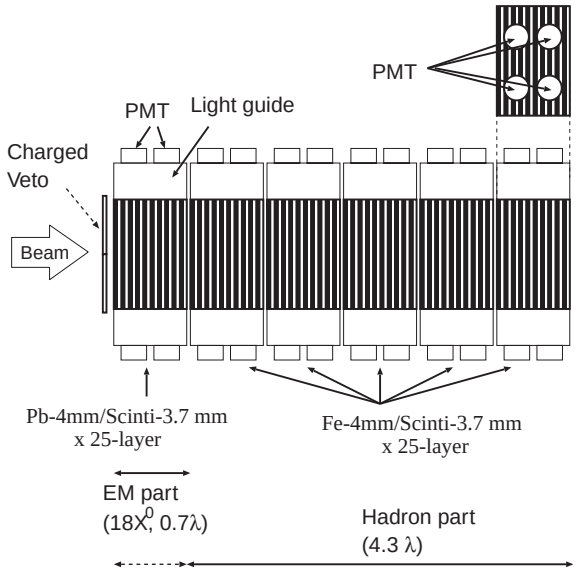

Fig. 10. Schematic side view of the hadron calorimeter "Cerberus". Cerberus consists of 6 modules. The first module is a sandwich of 25 layers of Pb(4 mm)/Scinti(3.7 mm). The other modules are sandwiches of 25 layers of Fe(4 mm)/Scinti(3.7 mm). The cross-section of the sensitive part is $40 \times 40\,\mathrm{cm}^2$.

A Monte-Carlo simulation code based on the G-FLUKA package in the GEANT-3 program was used for a detector simulation. We obtained the energy deposition in the scintillators for neutrons and γ's event by event.

In order to separate γ's and neutrons, we defined a parameter "F/T", which is the ratio of the energy deposition in the first module and the total modules. We applied a cut of $F/T<0.5$ for a neutron and $F/T>0.85$ for a γ. For these conditions, the detection efficiencies for 1-GeV particles were calculated by the simulation; the results are given in Table 2.

4.2.2. Results

Fig. 11 shows the energy distributions for the neutrons and for the γ's, respectively. The hatched histograms indicate the Monte-Carlo results. The circles with error-bars indicate the experimental data. The data were reasonably well reproduced by a Monte-Carlo simulation. The Monte-Carlo results for γ with the Pb-absorber and no-absorber were slightly under-estimated and over-estimated,

respectively. Since there was contamination of neutrons in the γ signals, as shown in Fig. 11, these deviations might be caused by incorrect particle identification. However, they were within a factor of 2.

Table 2
Typical detection efficiencies of "Cerberus" estimated by a simulation based on the GEANT-3 program

	Neutron (%)	γ (%)
$F/T<0.5$	73.8	0.1
$F/T>0.85$	8.4	99.5

Particles were generated at the center of the detector with a kinetic energy of 1.0 GeV. Definitions of "F/T" are given in the text.

By inserting the Pb absorber, γ decreased to 0.20%, while the neutrons decreased to 60.9% in the energy region above 1 GeV. In the case of the Be absorber, γ's and neutrons decreased to 50.7% and to 34.9%, respectively.

Fig. 12 shows a comparison of the energy distributions between the halo region and the core region for the no-absorber case. The number of events was normalized to 10^{10} protons on the target. The maximum energy in the halo region was about half of that in the core region. The ratios of the number of events between the halo and core regions above 0.5 GeV were 3.54×10^{-4} at 35 cm and 1.32×10^{-4} at 80 cm for neutrons, and were 3.90×10^{-4} at 35 cm and 0.66×10^{-4} at 80 cm for the γ's. These ratios are qualitatively

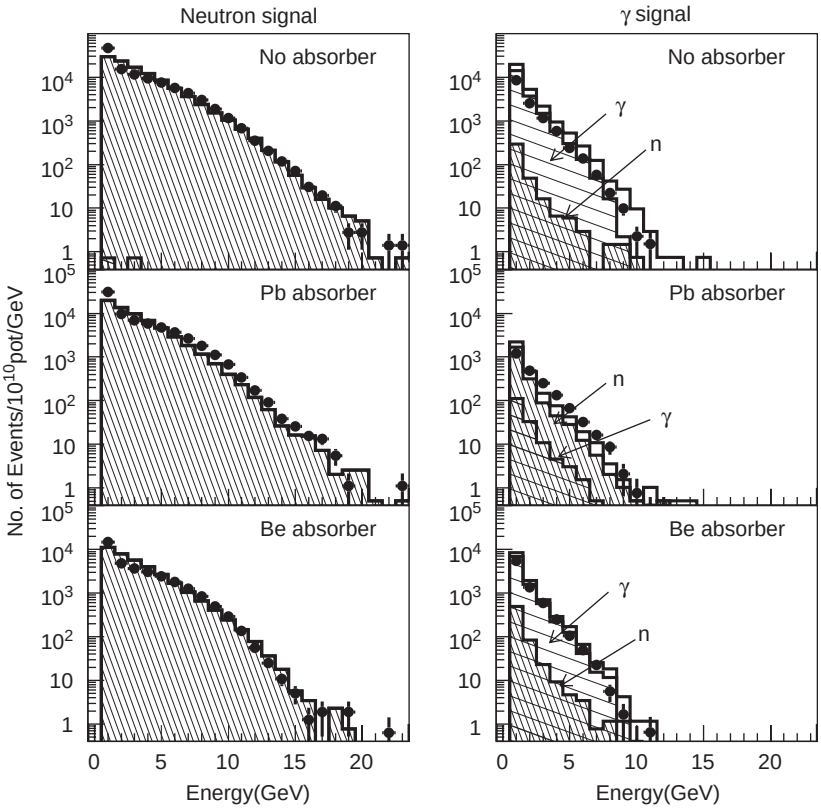

Fig. 11. Energy distributions of neutrons(left) and γ's(right) measured by Cerberus. The circles with error-bars indicate the experimental data. The both open and hatched histograms show the Monte-Carlo simulation. The densely-hatched histogram indicates the contributions from neutron events, and the sparsely-hatched histogram indicates the contributions from γ events. The condition of the beam-line absorber is indicated in the figure.

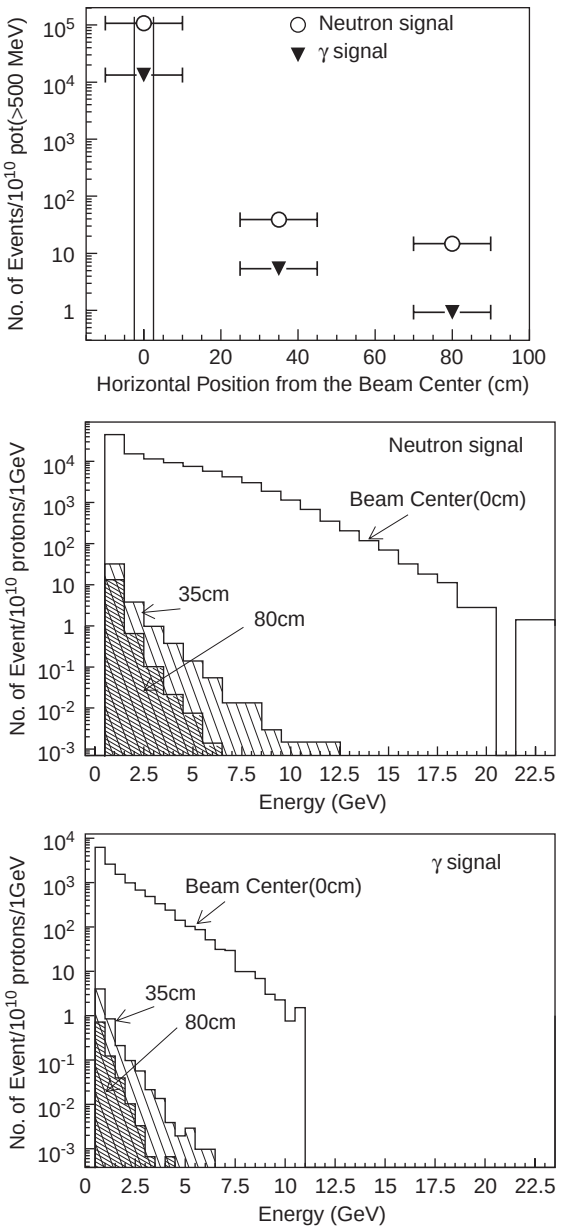

Fig. 12. Comparison between the energy distribution in the core region and that in the halo region for the no-absorber case. The top figure shows the number of events above 500-MeV deposition as a function of the distance from the beam axis. The lines show the beam-core region. The middle and bottom figures show the spectrum for neutrons and γ's, respectively. The sparsely-hatched histogram shows the data at 35 cm from the beam axis. The densely-hatched histogram shows the data at 80 cm from the beam axis.

consistent with the profile measurements described in the previous section.

4.2.3. Thermal neutron flux

Thermal neutrons could be one of the main sources of the single rate of the detectors surrounding the K_L^0 decay region. Therefore, reducing the thermal-neutron flux is very important in the $K_L^0 \to \pi^0\nu\bar{\nu}$ experiment.

A ^{6}LiI(Eu) scintillation crystal was used as a thermal-neutron detector. It has a dimension of 1 inch-ϕ and 2 mm thick. When a ^{6}Li-nucleus absorbs a thermal neutron, the following reaction occurs:

$$^6_3\mathrm{Li} + ^1_0\mathrm{n} \to ^4_2\alpha + ^3_1\mathrm{H} + 4.7\,\mathrm{MeV}.$$

The Q-value of this reaction is 4.7 MeV. Since the cross-section is 940 barn at the thermal energy, the detection efficiency of the 2 mm-thick ^{6}LiI(Eu) scintillator is 95%.

Fig. 13 shows the energy spectra measured with the ^{6}LiI(Eu) scintillator in the second beam survey, after installing the Gd_2O_3 sheets at C4, as described in Section 2.3.1. Thermal-neutron events are clearly seen as a peak around 4 MeV, especially in the halo region. A Landau distribution around 1.2 MeV corresponds to minimum-ionizing particle(MIP) events from the beam. The ratio of peak positions is about 3.5, as expected for the thermal-neutron and the MIPs. The number of thermal-neutron events was estimated after fitting the spectra with Gaussian + exponential. Fig. 14 shows the thermal-neutron fluxes as a function of the detector position. The effects of the Gd_2O_3 sheets can be clearly seen. They reduced the thermal-neutron flux by one order of magnitude. The Be absorber reduced the thermal-neutron flux by a factor of 2.

5. Summary and discussion

A neutral beam line was constructed at the 12-GeV proton synchrotron of KEK in order to provide a "pencil" and "clean" K_L^0 beam for the E391a experiment. After a series of beam-survey experiments, it was confirmed that the two-stage beam collimation system works properly.

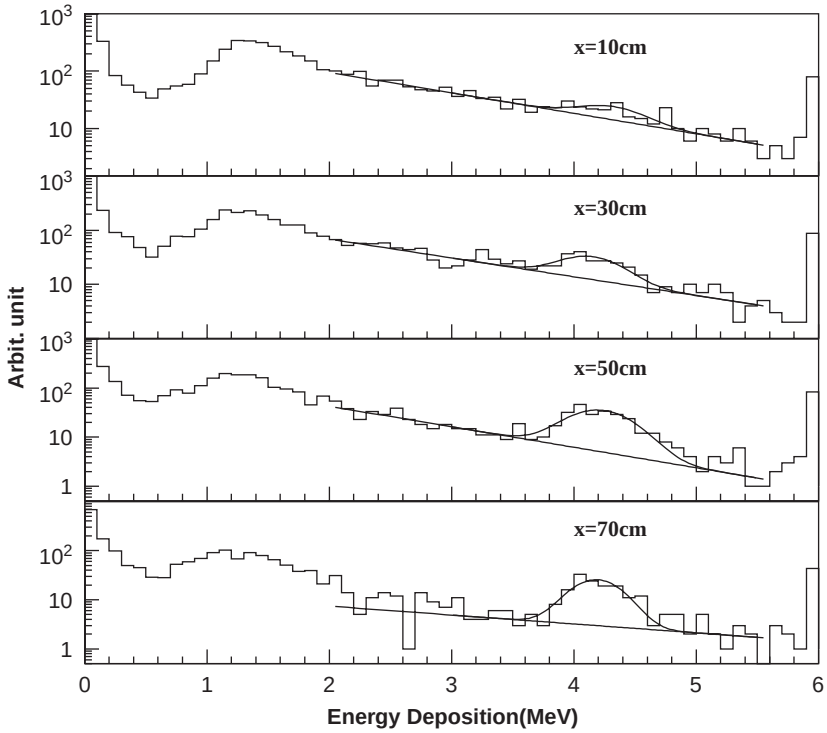

Fig. 13. Energy spectra measured with the LiI(Eu) scintillator after the installation of Gd_2O_3 absorbers and the primary beam-dump plug. X in the figure is the distance from the beam axis. Thermal-neutron events are clearly seen as a peak at 4 MeV. A Landau distribution around 1.2 MeV corresponds to minimum-ionizing particle(MIP) events from the beam.

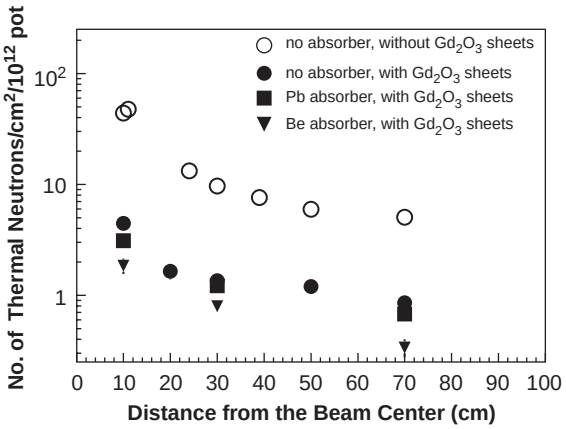

Fig. 14. Thermal-neutron fluxes in the detector area. The open circles and closed symbols indicate the fluxes before and after the installation of Gd_2O_3 absorbers and the beam-dump plug, respectively. The Gd_2O_3 absorber gives the reduction of the thermal-neutron flux by one order of magnitude. The square and triangle indicate the results for the case with the Pb absorber and Be absorber in the beam line. By using the Be-absorber, the thermal-neutron flux is reduced by a factor of 2.

The observed beam profiles and the energy spectra of γ's and neutrons were fairly well reproduced by Monte-Carlo simulation. This fact encourages us to further improve the quality of the neutral beam through Monte-Carlo simulation studies.

As for the K_L^0 beam, we only present here the result of a simulation for the K_L^0 flux and the momentum distribution. These will be measured by the E391a experiment through the detection of such decay modes as $K_L^0 \to \pi^0\pi^0\pi^0, \pi^0\pi^0$, and $\gamma\gamma$. The result will be reported later.

Acknowledgements

The authors would like to thank the staff of the beam channel group of KEK-PS for providing us with the EP-2 beam line and the K0 beam line. The authors would like to thank all members of the E391a collaboration for their help and valuable

discussions. This work was partly supported by a Grant-in-Aid for Scientific Research of the Ministry of Education, Science, Sports and Culture of Japan.

References

[1] G. Buchalla, A. Buras, M. Lautenbacher, Rev. Mod. Phys. 68 (1989) 1125.

[2] T. Inagaki, et al., Measurement of the $K_L^0 \to \pi^0 \nu\bar{\nu}$, KEK Internal, 96-13, 1996.

[3] K. Abe, et al., Status of the $K_L^0 \to \pi^0 \nu\bar{\nu}$ experiment at KEK, KEK Preprint, 2000-89, 2000.

[4] A. Alavi-Harati, et al., Phys. Rev. D 61 (2000) 072006.

[5] CERN Application Software Group, GEANT-Detector Description and Simulation Tool, W5013, CERN, 1993.

[6] T. Sato, Beam and target monitor using thermocouples, Proceedings of ICANS-XV, KEK-Proceeding, vol. 2000-22, 2001, p. 308.